Full Length Research Article

FIELD ION MICROSCOPY THE MODIFICATION OF THE ATOMIC STRUCTURE OF THE MATERIALS AFTER STRONG EXTERNAL EXPOSURES

Ivchenko, V. A.

Yeltsin Ural Federal University, Ul, Mira 19, Yekaterinburg, 620002 Russia
Institute of Electrophysics, Ural Branch, Russian Academy of Sciences, ul, Amundsena 106, Yekaterinburg, 620016 Russia

---

ARTICLE INFO

ABSTRACT

The paper presents the application of direct methods (field ion microscopy and atom probe techniques) to study the modification of the crystal structure of various materials at atomic spatial level after strong external exposures. On the original results shows the possibility of three-dimensional reconstruction of the elemental composition of the materials studied with atomic resolution to study the modification of the atomic structure. It is established that the nature of the crystalline structure of the boundary region of planar defects depends directly on the type of external influence.

INTRODUCTION

Among the most efficient and advanced methods for studying conducting and semiconducting materials, using which the lattice of solids can be directly studied with atomic spatial resolution, are field ion microscopy (FIM) and various modifications of atom probes of a field ion microscope. The objective of this paper is to demonstrate the efficient use of atom probe methods for studying nano structured states arising in the bulk of metals and alloys during modification of the atomic structure of various materials by strong external exposures. It is shown that, along with the lattice distortions typical of thermo mechanical, thermal, strong deformational, and other perturbations (dot, linear, dislocation, and other lattice defects are meant), the studied materials contain such radiation defects as vacancy clusters, amorphized regions, and nano segregations of atoms of one of the components in ordered alloys. The microscope field size (~100 nm) and an analysis of the sample volume by controlled layer by layer evaporation of surface atoms make it possible to determine whether the material under study is nanostructured or not.

*Corresponding author: Ivchenko, V. A.
Yeltsin Ural Federal University, ul. Mira 19, Yekaterinburg, 620002 Russia, Institute of Electrophysics, Ural Branch, Russian Academy of Sciences, ul, Amundsena 106, Yekaterinburg, 620016 Russia.

The possibility of studying the sample in a volume down to micron sizes makes it possible to obtain macro scale experimental data. FIM is the only microscopy technique capable of providing direct observation of individual atoms as elements composing the sample structure during an ordinary experiment. The use of FIM makes it possible to select an individual atom in the image for mass spectrometric identification (atom probe FIM methods), to perform in situ experiments with individual atoms deposited on the surface, and to reconstruct the structural and chemical compositions in the sample volume by controlled layer by layer removal of surface atoms by an electric field at cryogenic temperatures. Exactly the latter situation distinguishes direct FIM methods from other structurally sensitive ones with atomic resolution, but being indirect methods of microscopic study of materials.

MATERIALS AND METHODS

The samples to be studied were prepared as tip emitters with an apex curvature radius of 30–50 nm from materials preliminarily processed by various strong external exposures, i.e., electrochemically polished wires or rods. Objects of the interaction with accelerated beams of gas ions ($E = 20$ keV, implantation dose $D = 10^{13}–10^{18}$ ion/cm^2, and current density $j = 100–340$ μA/cm^2) were various metal materials.

Field emitters certified for ion implantation were characterized by an atomically smooth surface of the apex prepared by in situ field evaporation of surface atoms. In Fig. 1. shows ion image of Pt after certification. On the one hand, micro pattern represents the contrast of the tip end surface from atoms in the step edges; on the other hand, it reflects the stereographic projection of the crystal under study. Circular contour lines in the ion image are edges of corresponding sets of crystallographic planes of certain directions. Adjacent rings (from any set of concentric rings) represent images of parallel atomic layers. The distance between rings corresponds to the interplane distance for a given crystallographic direction. In terms of the ion microscopic picture, this distance is also referred to as the lattice step height. The rings themselves in the ion microscopic picture, as a rule, consist of isolated bright dots which are images of surface atoms arranged at atomic sites in step edges.

Fig. 1. Neon image of Pt single crystal, $U = 10$ kV

Materials such as Cu80Co20 were mechanical alloyed by high purity (99.9%) Cu and Co powders with particle sizes of ~50 μm. Powders were treated in a centrifugal planetary mill in an argon atmosphere at room temperature for 20 h. The ratio of steel balls of the mill to powder particles was 1: 25. After mechanical alloying, powders were compacted into pellets by compression shear at 500 MPa. Some pellets were annealed at 400°C for 2 h. Work pieces for future pins were rods (~0.2 × 0.2 × 10 mm^3 in volume) cut from thermally treated pellets by spark cutting. All atom probe FIM (APFIM) and tomographic atom probe (TAP) studies were performed with the ratio of the pulse voltage to the dc voltage of 20% and a repetition rate of 775 Hz in high vacuum (1×10^{-8} Pa). The sample temperature during measurements was 60–80 K.

RESULTS AND DISCUSSION

The objects of interaction with accelerated beams of gas ions were pure metals (Ir), atomically ordering alloys (Cu3Au), and solid solutions (50Pd30Cu20Ag) whose decomposition results in an atomically ordered phase separation (Ivchenko and Syutkin, 1999; Bunkin *et al.*, 1990; Bunkin *et al.*, 1990; Ivchenko and Syutkin, 1995; Ivchenko *et al.*, 1988; Ivchenko *et al.*, 2000; Ivchenko *et al.*, 1997). Using the FIM method, the effect of partial amorphization in the subsurface volume of tomically ordered alloys due to implantation of positive argon ions accelerated to 20 keV ($D = 10^{18}$ ion/cm^2 and $j = 200$ μA/cm^2) (Ivchenko *et al.*, 2000) was detected.

Partial amorphization was observed at distances no less than 90 nm from the irradiated surface of materials. Only the beam current density was varied in the experiment; the implantation energy and dose were unchanged ($E = 20$ keV, $D = 10^{18}$ ion/cm^2). At $j = 275$ μA/cm^2, a structural phase transition occurred in the entire material volume, which indicated sample heating to the critical temperature of phase transformation (~390°C), and the cooling rate corresponded to the conditions of the transition to the disordered state. During irradiation with a beam with $j = 250$ μA/cm^2, no structural phase transformation was observed, since accelerated argon ions did not heat the sample to the critical temperature. Therefore, the structure state of ordered Cu3Au alloy was studied after irradiation at $j = 200$ μA/cm^2, which a priori pointed to a low sample temperature during ion implantation.

After ion implantation ($j = 200$ μA/cm^2) of the ordered alloy, unstructured atomic arrangement in surface layers was observed, Fig. 2. An analogue of such ion contrast corresponded to the ion contrast of amorphous materials obtained by ultrafast cooling. Such a structure state appeared in the subsurface volume at distances of up to 90 nm from the irradiated surface. It is known that argon ions accelerated to 20–25 keV are characterized by a projected range in individual alloy components no longer than a maximum of 15 nm (Burenkov *et al.*, 1985). Therefore, it is clear that the phenomenon of partial amorphization in the subsurface volume of Cu3Au alloy cannot be explained by implanted argon ions. With the aim of studying the atomic structure of defects formed in the regions of single displacement cascades, the atomically ordered Cu3Au alloy was irradiated normally to the tip sample axis ($E = 40$ keV, $j = 10^{-3}$ A/cm^2, implantation duration $t = 10^{-3}$ s, $D \sim 6 \times 10^{12}$ ion/cm^2).

This provided incidence of, on average, one ion on a surface area of 4×4 nm^2. An analysis of the obtained ion microscopic pictures of the surface detected such radiation damage as disordered regions (DRs) and copper atom segregation (Bunkin *et al.*, 1990). The average DR size determined by the results on samples was $4 \times 4 \times 1.5$ nm^3. The DRs were identified as violations in the circular contrast pattern on the atomically ordered alloy surface whose contrast is similar to the ion contrast of the pure metal surface, since it is caused only by gold atoms in ordered Cu3Au alloy. Such contrast was retained during field evaporation of surface atoms to the DR depth. The experimentally determined average DR size was in order of magnitude agreement with the calculated diameter of the displacement cascade (5–11 nm), which was estimated as the mean range of the surface implanted atom in the approximation of a sphere shaped cascade region. The actual size of cascade regions (taking into account the mean range of atoms knocked out from the core of the cascade of atoms occupying interstices and not always reliably identified by the FIM method) was probably slightly larger than the experimentally measured one. The study detected only copper atom segregations (Bunkin *et al.*, 1990). Since copper atoms do not yield a visible image on ion micrographs of the surface, the contrast from the copper segregation is observed as a dark area. Clusters or segregations of copper atoms are three dimensional and contain, as a rule, 200–500 atoms.

It is almost impossible to experimentally determine the presence of vacancies in these clusters, although the analysis of the ion contrast of dark area boundaries shows that their possible number is insignificant. The study of ion implanted PdCuAg detected the phase structural transition in its subsurface volume (Ivchenko *et al.*, 1995). The size of the surface volume in which the structural phase transformation was detected was estimated as a function of the beam current density. In the subsurface volume, vacancy clusters (micropores) were detected, Fig.3, and their sizes and shape were estimated. Micropores were shaped as ellipsoids 4–25 nm high and 3–12 nm in diameter. The volume fraction of micropores monotonically decreases with the distance from the irradiated surface. Thus, the interaction of charged gas ion fluxes with metals and alloys in implanted materials results in a defect structure which can be caused by the effect of only the irradiation process. In addition to point, linear, dislocation, and other lattice defects which are typical of external exposures (thermomechanical, thermal, deformational), such radiation damage as vacancy clusters, amorphized regions, segregations of atoms of one of the components in ordered alloys, and disordered regions is observed in the studied ion implanted metals and alloys.

The FIM study of the structure of metals subjected to intense plastic deformation showed different atomic structures of their planar defects in comparison with those detected after implantation. For example, after intense plastic deformation (IPD) by packet hydroextrusion in coarse_crystalline nickel (logarithmic strain $e \approx 12$), a submicrocrystalline (SMC) state (the average microcrystallite grain size $dg \approx 100$ nm) was formed (9). As a result, ultradisperse subgrains were detected, whose sizes were estimated both on the nickel SMC surface and during removal of one atomic layer after another at ~3–10 nm. An analysis of the ion contrast showed that subgrain bodies are perfect microcrystallites hardly misoriented with respect to each other. During the study of the atomic structure of SMC nickel, emergences of individual dislocations at subgrain interfaces were observed. The boundary region width was comparable to the interatomic distance.

The atomic structure of planar defects was studied in metallic tungsten (99.99% pure W) upon severe plastic deformation. A submicron grained structure in the metal was obtained using high plastic deformation up to a true logarithmic exponent of $e = 7$ by torque under quasi hydrostatic pressure in a Bridgman anvil type device. Another sample material was polycrystalline nickel (99.96% pure Ni grade) deformed under pressure by the method of packet hydroextrusion (PHE) at room temperature. For obtaining nickel samples with various degrees of grain refinement, the initial 6 mm diameter rods upon a single stage PHE at the relative deformation up to 80% were annealed in a temperature interval of $T = 450$–1000°C for the corresponding periods of time. The ultrafine grained structure was obtained in nickel samples with initial grain size $d \approx 8$ μm by multistage PHE route to a true logarithmic exponent of $e = 12$. The investigation of mechanically deformed iridium samples revealed a high density of point, linear, and volume structural defects. A comparative analysis of planar defects (Ivchenko and Syutkin , 1999) observed in pre deformed (~90%) and irradiated iridium showed a significant difference between their structures.

The mechanically deformed iridium consisted of grains with dimensions within 20–30 nm, the bodies of which were almost free of structural defects. In contrast, the ion irradiated ($E = 20$ keV, $D = 10^{18}$ ion/cm^2, $j = 300$ μA/cm^2) metal exhibited a subblock microstructure with a characteristic size of ~3–5 nm, block misorientation within 0.5°–1°, and various defects in the bodies of blocks.
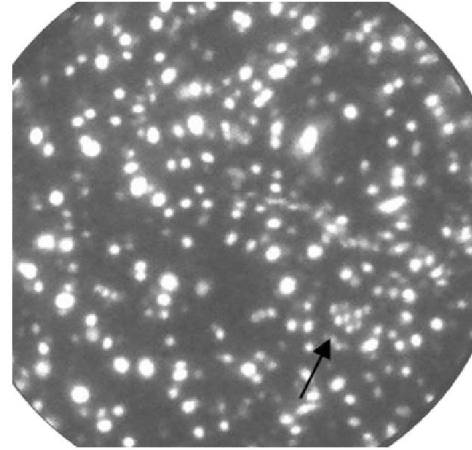
Fig. 2. Ion pattern of Pt surface after irradiation by Ar+ with D = 10^{18} ions/cm2 (T = 300°C) (the arrow denote the region of the crystalline state of the metal)
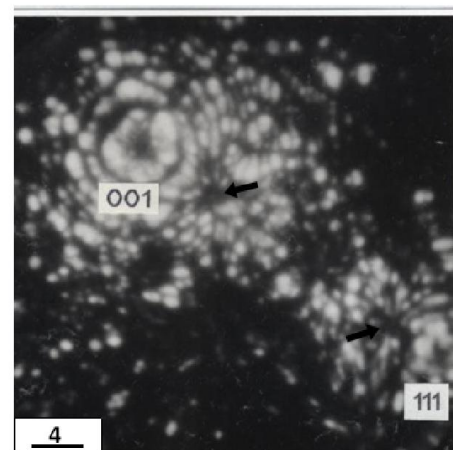
Fig. 3. A region of ion contrast of ion-implanted alloy 50Pd30Cu20Ag, after the removal of 14 atomic layers of the irradiated surface (arrows show ion contrast micropores)

The width of boundary regions at interfaces in samples upon various external actions was, similarly to heat treated metals and alloys, on the order of interatomic distances. The boundary region width significantly changes in the case of materials obtained by mechanical alloying (Fig. 2) (Ivchenko *et al.*, 2000). Figure 4a shows a three dimensional (3D) reconstruction of the elemental map of mechanically alloyed Cu80Co20 compound. Determination of the composition of annealed material revealed three regions with different concentrations of cobalt: (a) a region containing 8.7 at % Co, (b) an intermediate region containing 32.5 at % Co, and (c) a region with high Co concentration and only 1.3 at % Cu. All these regions exhibit interphase boundaries with an effective width of about 1.5 nm (Fig. 4b). The plot in Fig. 4b shows variation of copper content in the boundary regions of interphase interfaces.

The FIM study of nickel samples clearly revealed the boundaries of ultradisperse blocks, which constitute the microstructure of individual grains (Ivchenko *et al.*, 2003). The dimensions of blocks, which were estimated both on the surface FIM image and in the course of controlled sequential removal of surface atomic layers, varied from 1 to 10 nm. It was established that the bodies of blocks comprise perfect crystallites that are almost not misoriented relative to each other.
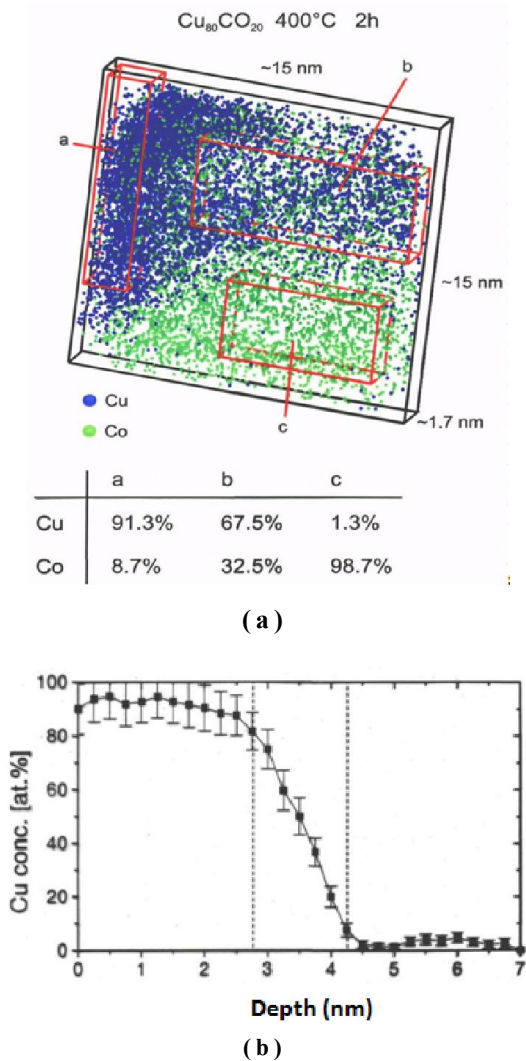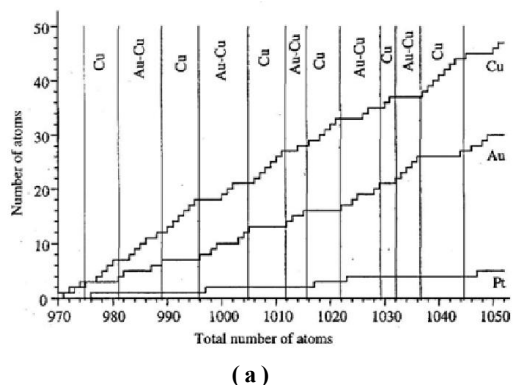

	a	b	c
Cu	91.3%	67.5%	1.3%
Co	8.7%	32.5%	98.7%

(a)

(b)

Fig. 4. (a) 3D elemental map of mechanically alloyed Cu80Co20 compound (upon annealing at 400°C for 2h) as reconstructed by TAP data; (b) interphase boundary width of mechanically alloyed Cu80Co20 compound upon 2 h annealing

(a)

	In the volume	Near the boundary	At the boundary	Actual
Cu	65.0 ±3.4	54.9 ±2.4	42.9 ±3.3	7
Au	26.6 ±1.3	38.1 ±2.3	49.5 ±2.8	2
Pt	5.4 ±0.6	7.0 ±1.2	7.5 ±1.5	4
Total number of ions	1224	428	331	
Au/Pt	5.48(+0.96-0.76)	5.44(+1.52-1.08)	6.56(+2.16-1.37)	6

(b)

Fig. 5. (a) Part of a step diagram obtained by APFIM analysis of (001) face of Cu3Au alloy with Pt impurity (vertical lines separate steps of anticipated width corresponding to the results of layer by layer analysis and a calculated radius of curvature of the point tip; (b) composition of Cu3Au alloy (with 4 at % Pt) determined by APFIM in comparison to the actual concentrations of components

The investigation of atomic structure showed evidence of the emergence of separate dislocations at the interfaces of blocks. The widths of boundary regions were on the order of the interatomic distance. To the first approximation, the obtained data are identical to the results of atomic structure investigation in submicrocrystalline (SMC) tungsten (with an average grain size of ~100 nm) upon severe plastic deformation ($e \approx 7$) (Mulyukov *et al.*, 2000). An analysis of the FIM images of an SMC tungsten surface region with a grain boundary showed that its width was about 0.6–0.8 nm. It should be noted that the boundary width in the initial coarse_grained tungsten amounted to 0.3–0.4 nm (Ivchenko . and Syutkin, 1999). In addition, the use of field electron microscopy (FEM) and electron spectroscopy techniques revealed significant differences between the electron energy distributions in SMC and coarsegrained tungsten (Mulyukov *et al.*, 2000). The ion contrast of the boundaries of ultrafine grains in copper upon severe plastic deformation showed evidence of a wider boundary region (on the order of three to four interatomic distances).

In addition, the ultrafine (8–15 nm) grains in a torque deformed material exhibited a strong mutual misorientation. The atomic_probe investigation of the influence of distribution of platinum atoms on the strength of ordered Cu3Au4 alloy (containing 4 at % Pt) was performed by APFIM with a time of flight mass spectrometer (Ivchenko *et al.*, 1996). A lower evaporation field of Cu relative to those of Au and Pt hindered the atomic probe analysis, since, even at $T = 28$ K and a 15–20% ratio of pulse amplitude to bias voltage on the emitter, it was impossible to avoid preferential evaporation of copper at a constant bias voltage. This negative effect was even more pronounced on grain boundaries, from which more gold atoms than copper atoms reached the detector. With allowance for the preferential field evaporation of copper atoms, it was possible to determine the concentration of doping impurity atoms in the material. As a result, it was found that the content of Pt atoms in the alloy studied amounts to 4 at % in the bulk and is close to this value at the grain boundaries. Fig. 5a shows a step diagram constructed by APFIM data, from which it seen that Pt atoms occupy the crystalline lattice sites in both Au–Cu and purely Cu layers on the (0001) face. It should be recalled that purely copper layers are not imaged by FIM. Note that Fig. 5a shows only a part of the entire diagram obtained during the atomic probe analysis of alternating Au–Cu and purely Cu layers in the alloy sample. The total number of ions evaporated in the given experiment amounted to 2003.

Results of microanalysis in the vicinity of and immediately on the boundary (identified as a twin boundary) are summarized in the table (Fig. 5b). Based on the obtained results, it was concluded that Pt atoms occupy at statistical probability the crystalline lattice sites of the ordered alloy. Therefore, the alloying of Cu_3Au with Pt ensures solid solution strengthening of the $L1_2$ superstructure.

Conclusion

Thus, application of direct methods for studying the crystal structure of various materials at the atomic spatial level (field ion microscopy and atom probe FIM methods) after various intense external exposures was demonstrated. For example, the effects of amorphization of subsurface volumes of alloys, deformation effects in pure metals, and structural phase transformations in subsurface volumes of solid solutions were detected during radiation exposure to charged particle beams with an energy of 20 keV.

It is established that the nature of the crystalline structure of metal interfaces significantly depends of the type of external action and determines eventually the physical (in particular, mechanical) properties of materials. Experimental data on the elemental composition of interphase interfaces in mechanically alloyed compounds and doped alloys have been obtained. It is established that the width of boundary regions at metal interfaces vary within 0.8–1.5 nm depending on the type of intense external action to which they were subjected.

Acknowledgements

REFERENCES

Bunkin, A. Yu., Gavrilov, N.V., Ivchenko, V. A., *et al.* 1990. *Fiz. Met. Metalloved.*, vol. 69, no. 4, pp. 171–175.

Bunkin, A. Yu., Ivchenko, V.A., Kuznetsova, L. Yu., *et al.* 1990. *Fiz. Met. Metalloved.*, vol. 69, no. 7, pp. 111–318

Burenkov, A.F., Komarov, F.F., Kumakhov, M.A., and Temkin, M.M. 1985. Spatial Distributions of the Energy Released in Atomic Collision Cascades in Solids, Moscow: Energoatomizdat.

Ivchenko V. A. and Syutkin N. N. 1999. Tech. Phys. Lett. 25 (3), 233.

Ivchenko, V. A., Efros, B. M., Popova, E. V., Efros, N. B., Loladze, L. V. 2003. Fiz. Tekh. Vys. Davlen. 13 (3), 109.

Ivchenko, V. A., Kvist A., Andren H. O., *et al.* 1996. Appl. Surf. Sci. 94/95, 267.

Ivchenko, V., Wanderka, N., Czubayko, U., Naundorf, V., Ermakov, A. Ye, Yimin, M. A. and Wollenberg, H. 2000. Mater. Sci. Forum 343/346, 709.

Ivchenko, V.A. and Syutkin, N.N. 1999. *Pis'ma Zh. Tekh. Fiz.,* vol. 25, no. 6, pp. 60–64.

Ivchenko, V.A. and Syutkin, N.N.1995. *Appl. Surf. Sci.*, vol. 87/88, pp. 257–263.

Ivchenko, V.A., Efros, B.M., Popova, E.V., *et al.* 2003. *Fiz. Tekh. Vysok. Davlen.,* vol. 13, no. 3, pp. 109–116.

Ivchenko, V.A., Ovchinnikov, V.V., Goloborodsky, B.Yu., and Syutkin N.N. 1997. *Surf. Sci.,* vol. 384, pp. 46–51.

Ivchenko, V.A., Syutkin, N.N., and Bunkin, A. Yu., *J. Phys (Paris)*, vol. 49_C6, pp. 379– 383.

Ivchenko, V.A., Syutkin, N.N., and Kuznetsova, L.Yu., 2000. *Pis'ma Zh. Tekh. Fiz.,* vol. 26, no. 13, pp. 5–10.

Mulyukov, R. R., Yumaguzin, Yu. M., Ivchenko, V. A. and Zubairov, L. R. 2000. JETP Lett. 72 (5), 257.

****